Journal of Physics and Chemistry of Solids 70 (2009) 576–583

Contents lists available at ScienceDirect

Journal of Physics and Chemistry of Solids

journal homepage: www.elsevier.com/locate/jpcs

Probing the microstructure of cement mortars through dielectric parameters' variation

C. Tsonos [a,*], I. Stavrakas [b], C. Anastasiadis [b], A. Kyriazopoulos [c], A. Kanapitsas [a], D. Triantis [b]

[a] Department of Electronics, Technological Educational Institute of Lamia, 35100 Lamia, Hellas, Greece
[b] Department of Electronics, Technological Educational Institution of Athens, 12210 Athens, Hellas, Greece
[c] Department of Civil Engineering, Technological Educational Institution of Athens, 12210 Athens, Hellas, Greece

ARTICLE INFO

Article history:
Received 23 July 2008
Received in revised form
15 December 2008
Accepted 17 December 2008

Keywords:
A. Microporous materials
D. Dielectric properties
D. Electrical conductivity
D. Electrical properties
D. Microstructure

ABSTRACT

The present work deals with the electrical properties of typical cement mortars during the hardening process, cured at low relative humidity. Measurements were made by using dielectric spectroscopy (DS) over a broad frequency range of 10 Hz–1 MHz and isothermal depolarization current (IDC) techniques, for several weeks after sample preparation. This work presents a coherent study of the various formalisms employed in dielectric spectroscopy. Each of these formalisms contributes to the development of the complete relaxation mechanisms that are responsible for the frequency spectrum. After the first week of hardening, when the DC conductivity effects were absent, two distinct dielectric relaxation mechanisms were observed in the frequency spectrum of the complex permittivity ε^* and $\tan\delta$ functions. The mechanism positioned at low-frequency region (few kHz) is observed for the first time, as we know from the literature, on cement mortars. The relaxation times of both mechanisms were found to increase gradually, while the strength of the relaxation mechanisms varied also as a function of the hardening time. Fitting analysis in complex impedance Z^* and electric modulus M^* formalisms revealed also the existence of two short-range relaxation mechanisms of conductivity. We suggest that the low-frequency relaxation is related to the closed capillary pores and the high-frequency relaxation to the C-S-H gel pores. An increase of the mean dimension, of both types of pores, estimated from our data analysis with hardening time.

1. Introduction

Cement-based materials, like mortars and concretes, dominate in the construction field. Portland cement mortar is a porous, chemically bonded ceramic, which results from the reaction of an initial suspension of Portland cement powder, sand and water. Portland cement consists primarily of calcium silicates, with fairly small amounts of aluminates, ferrites and sulphates [1]. The hydration reaction between tricalcium silicate (C_3S) and dicalcium silicate (C_2S) with water leads to the formation of a poorly crystalline or amorphous calcium silicate hydrate, commonly referred to as C-S-H gel. C_3S is associated with the hardening reaction occuring during the early stage of hydration that happens within the first few weeks. The slower-reacting C_2S continuously develops the strength for months or more. Another important phase is calcium hydroxide, CH, which forms crystals. The growth of C-S-H gel, during the hardening process, operates as a bridge between the individual particles of cement sample and leads to the formation of pores filled with conductive fluids of the reaction products whose dimensions range from nanometer scale to millimeter scale. The volume of the cement samples, termed capillary pores, originally contained a conductive fluid. These pores reduce in size and become increasingly tortuous. Pores in nanometer scale are contained within C-S-H gel. Porosity and the distribution of pore sizes control the mechanical properties of cement samples.

Dielectric spectroscopy (DS) measurements have been used to study the microstructure of materials based on cement [2–7] and other minerals [8,9]. DS is a technique in which an alternating voltage at a single frequency is applied to a sample, and the magnitude and the phase of current are measured [10]. DS measurements can be performed rapidly and easily without altering the microstructure of the sample. The work done in this area of interest is concentrated on neat cement paste, mortars and concretes, with attention focused on the hardening process and the early stage of hydration [3,11–13]. The electric properties of materials based on cement vary with time for months after sample preparation. It has been shown that the amount of water and sand and their interaction with the C-S-H environment deeply affect the dielectric response of the material [4].

Curing in high relative humidity environment results in high values of DC conductivity especially during the early stage of

* Corresponding author. Tel.: +30 22 3106 0277.
E-mail address: tsonos@teilam.gr (C. Tsonos).

0022-3697/$ - see front matter © 2008 Elsevier Ltd. All rights reserved.
doi:10.1016/j.jpcs.2008.12.015

hardening process on cement-based materials. In this case the contribution of conductivity masks every dielectric relaxation mechanism at the low-frequency range. DC conductivity is due to the ions motion in percolative pore channels inside the C-S-H gel phase. Dielectric dispersion in the high-frequency range, 1 MHz–20 GHz, has been attributed to water, structural, chemically bound, physically absorbed or free water [14–16]. Dielectric relaxation mechanisms in the low-frequency range, 1 kHz–1 MHz, have been attributed to interfacial effects [13,17,18]. Several models have been suggested to explain the low-frequency polarization mechanisms. Preparation and cure conditions have important influence on the electric and dielectric properties of cement-based materials.

In DS the stimulus is usually a voltage $V^*(\omega,t)$ (or a current $I^*(\omega,t)$) and the response is a current $I^*(\omega,t)$ (a voltage $V^*(\omega,t)$), where ω is the angular frequency $\omega = 2\pi f$, f is the frequency of the applied electric field and t is the time. Then, the transfer function of the measured system is the complex admittance Y^* or the complex impedance Z^*, which are related through Ohm's law through

$$Y^*(\omega) = \frac{1}{Z^*(\omega)} = \frac{I^*(\omega,t)}{V^*(\omega,t)}$$

The results of DS measurements can be described as functions of frequency via various formalisms, such as the complex permittivity $\varepsilon^* = \varepsilon' - i\varepsilon''$, electric modulus $M^* = M' + iM''$, complex impedance $Z^* = Z' - iZ''$, complex admittance $Y^* = Y' + iY''$, complex specific conductivity $\sigma^* = \sigma' + i\sigma''$ and dissipation factor or loss tangent $\tan\delta$. The DS formalisms are related to one another as follows:

$$M^* = \frac{1}{\varepsilon^*} \tag{1}$$

$$Z^* = \frac{1}{Y^*} = \frac{1}{i\omega C_o \varepsilon^*} \tag{2}$$

$$\sigma^* = i\varepsilon_o \omega\, \varepsilon^* \tag{3}$$

$$\tan\delta = \frac{\varepsilon''}{\varepsilon'} = \frac{M''}{M'} = \frac{Z'}{Z''} = \frac{Y'}{Y''} \tag{4}$$

where C_o is the geometrical capacitance, ε_o is the permittivity of vacuum and $i = \sqrt{(-1)}$. Choosing the proper formalisms makes it possible to reveal various details and aspects of dielectric and electrical response for a given system. Dipole polarization is usually described by the complex permittivity ε^*. Processes related to the motion of charge carriers are better described by the complex impedance Z^*, the complex electric modulus M^* and the complex specific conductivity σ^*. When conductivity is studied by DS the frequency dependence of the real part of complex specific conductivity is often considered because this dependence allows one to estimate the direct current (DC) specific conductivity σ_{dc}. The shape of the relaxation mechanisms in the complex plane or in a frequency dependence plot is described by various relaxation modes known as the Debye relaxation, Cole–Cole (C–C) relaxation, Davidson–Cole (D–C) relaxation and the Havriliak–Negami (H–N) relaxation [19].

The phenomena of polarization and depolarization are followed by currents through the sample polarization or depolarization currents, respectively. These currents may contain charge transport contributions from the bulk of the sample as well as charges injected from the electrodes. In many structures localized states of different origin may occur. The localized states may influence atom interaction and carrier motion.

Time domain analysis of depolarization or decay current processes can provide valuable information regarding the dielectric response of solids [20]. The time-dependent relaxation process following a sudden removal of a polarization field may be considered as a succession of four stages. During the relaxation, several mechanisms act concurrently each of them dominating the relaxation for a specific time [21,22]. The initial stage that is rather short ($t < 10^{-12}$ s) takes place immediately after removing the applied field. During the three of the rest stages the depolarization current can be described by the following laws [21]:

$$\begin{aligned} &i_d \propto t^{-n} && \text{for } t \ll 1/\omega_p \\ &i_d \propto \exp(-\omega_p t) && \text{for } t \cong 1/\omega_p \\ &i_d \propto t^{-m-1} && \text{for } t \gg 1/\omega_p \end{aligned} \tag{5}$$

The physical mechanisms with this behavior are clearly described in other works [21,22]. The depolarization mechanisms are mainly described by the factors n and m of Eq. (5). These factors describe the main active mechanism during each relaxation stage.

In this paper, we study the dielectric and electrical properties of cement mortar samples during the hardening process, at low relative environmental humidity. The aim of the present work is to examine the link between electrical response and the physicochemical processes occurring within the cement mortar by using different DS formalisms which give complementary information. According to the results presented below, curing of cement-based materials in a high relative humidity environment results in high conductivity values which mask relaxation mechanisms, especially in the low-frequency range (lower than 1 MHz). Indeed, the present study, which deals with samples cured under low-humidity environment, has identified a specific relaxation mechanism which otherwise would have been masked. In this respect, one of the merits of the present work is the fact that it studies relaxation mechanisms in realistically cured cement mortar samples. Many of the mechanical properties of cement-based materials depend on porosity. The present study has concluded on relaxation mechanisms, which can be attributed to the existence of pores. In that sense the electric measurements described below provide indirect information, concerning the pores of the material which is a necessary prerequisite for understanding and improving mechanical properties. Last but not least, the present application presents a coherent study of the various formalisms employed in DS. Each of these formalisms contributes in a consistent picture regarding the detailed relaxation mechanisms.

2. Experimental details

The cement mortar samples used in this work are composed of ordinary Portland cement (OPC), sand and distilled water at ratio 1:3:0.5. The maximum diameter of the sand grains was 2 mm, while the density and the porosity were 2.2 g/cm^3 and 8%, respectively. Two sets of samples with the same characteristics were individually prepared, one for the DS measurements and the other for the isothermal depolarization current (IDC) measurements. All samples were stored in plastic cases at room temperature (298 K) and at 40% relative humidity environment.

The DS measurements were conducted using an LCR meter (Agilent model 4284A), accompanied by the dielectric test fixture (Agilent model 16451B) and further supported by a computer for data recording, storage and analysis. Parallel capacitance (C_p) and loss tangent ($\tan\delta$) measurements of the palletized samples were performed with the LCR meter, in the frequency range 20 Hz–1

MHz. The detailed description of the experimental arrangement can be found elsewhere [23].

In order for the depolarization currents to be measured, a polarizing voltage $V_p = 1000\,V$ was applied for $t_p = 30\,min$. A Keithley 6514 programmable electrometer was used to perform the isothermal depolarization current measurements. DS and IDC measurements were carried out at room conditions within 6 weeks.

3. Results and discussion

The experimental results are discussed here and representative curves that correspond to both sets of the samples used for DS and IDC measurements are presented.

3.1. Dielectric spectroscopy technique

Fig. 1 shows the dependence of the imaginary part, ε'', of the complex dielectric permittivity ε^* on frequency f for different hardening times of the cement mortar. The contribution of the DC conductivity on the dielectric loss ε'' is reciprocal to the frequency f, i.e. it corresponds to the linear segment of lower frequency range, in the first week of hardening. In the higher frequency range a contribution from a dielectric relaxation mechanism is observed, which shifts gradually to lower frequencies as hardening time elapses.

Two distinct dielectric relaxation mechanisms are evident in Fig. 1 after the first week of hardening. The former appears at low frequencies (henceforth mentioned as LF) and the latter at high frequencies (henceforth mentioned as HF). Both mechanisms shift to lower frequencies as hardening time elapses.

The following expression was fitted to the experimental data of Fig. 1 [19]:

$$\varepsilon''(\omega) = \sum_{i=1}^{2} \frac{\Delta\varepsilon_i' \sin(\beta_i\varphi_i)}{[1 + 2(\omega\tau_{oi})^{1-\alpha_i}\sin(0.5\pi\alpha_i) + (\omega\tau_{oi})^{2(1-\alpha_i)}]^{\beta_i/2}} \tag{6a}$$

where

$$\varphi_i = \arctan\left[\frac{(\omega\tau_{oi})^{1-\alpha_i}\cos(0.5\pi\alpha_i)}{(1 + (\omega\tau_{oi})^{1-\alpha_i}\sin(0.5\pi\alpha_i))}\right] \tag{6b}$$

Eq. (6a) is the sum of Havriliak–Negami empirical equation and describes the contribution of the LF and HF mechanisms to the dielectric loss ε''. Parameters α ($0 \leqslant \alpha < 1$) and β ($0 < \beta \leqslant 1$) describe the deviations from the simple relaxation time. When $\alpha = 0$ and $\beta = 1$ the H–N equations coincide with the respective Debye equation. $\Delta\varepsilon_i'$ is the contribution of each mechanism to the real part of the dielectric function ε^* and $\tau_{oi} = 1/(2\pi f_{oi})$ is a characteristic relaxation time parameter, f_{oi} is the corresponding characteristic frequency that is closely related to each frequency where the dielectric loss ε'' has a maximum, f_{max}:

$$f_{max} = f_o\left[\frac{\sin\left[\frac{(1-\alpha)\pi}{2(1+\beta)}\right]}{\sin\left[\frac{(1-\alpha)\beta\pi}{2(1+\beta)}\right]}\right]^{(1/1-\alpha)} \tag{7}$$

All fits have been done using the non-linear least-squares Marquardt–Levenberg algorithm. From the fitting parameters, information can be derived for the time scale, the dielectric strength and the shape of dielectric relaxation mechanisms. However, only the dielectric strength and time scale will be discussed here.

Fig. 2 shows the plot of ε'' versus f with the respective best fit, for the 14th day of hardening. In the same figure the contributions of LF and HF mechanisms to the dielectric loss ε'' are also included. The LF mechanism presents f_{max} at 8 kHz on the 9th day of hardening, then it shifts to lower frequencies with respect to time (Table 1). The magnitude of the LF relaxation, $\Delta\varepsilon_L'$, also increases with time as shown in Table 1 (the subscripts "L" and "H" denote the low- and high-frequency processes, respectively). On the other hand, while HF relaxation becomes slower as hardening time increases, the magnitude $\Delta\varepsilon_H'$ progressively reduces (Table 1).

The variation of ε' versus frequency f on a log–log scale exhibits a plateau extending over a wide range of frequencies for

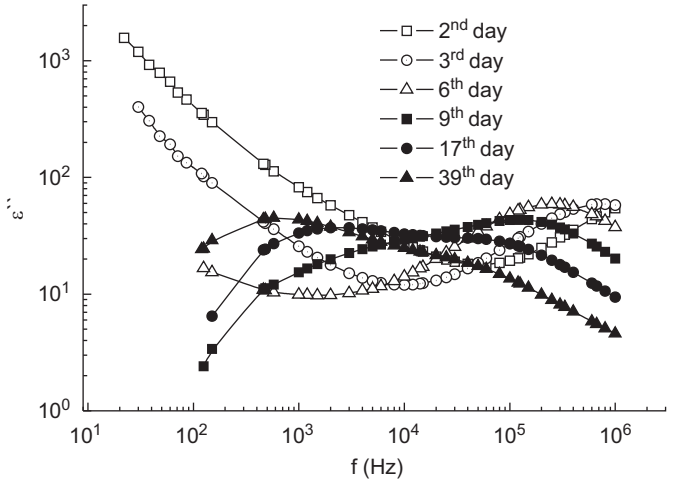

Fig. 1. The imaginary part of the dielectric permittivity versus frequency for several days of hardening.

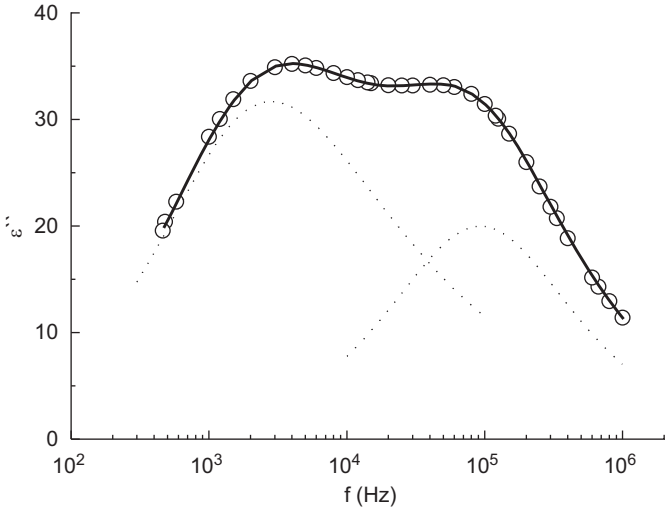

Fig. 2. The imaginary part of the dielectric permittivity versus frequency of cement mortar on the 14th day of hardening. The solid line is the best fit according to Eq. (6). The dotted lines show the contribution of the LF and the HF relaxations to the total spectrum.

Table 1
Parameters of the best fits of Eq. (6).

Day	$\Delta\varepsilon_L'$	$\Delta\varepsilon_H'$	$f_{max,L}$ (kHz)	$f_{max,H}$ (kHz)
9	98.2	80.5	8.03	147.23
14	117.0	55.0	3.07	92.75
17	131.8	38.4	2.40	79.65
24	141.9	26.7	1.66	65.00
39	149.7	17.7	0.73	41.13

measurements performed during the first 3 days of the hardening process (not shown here). The corresponding value of ε' is approximately 200. An increase of ε' values is observed at lower frequencies, during the first 3 days, which is due to the electrode polarization effect [24]. The dependence of ε' versus frequency f gives an evidence of the dielectric amplification, i.e. dielectric permittivity values larger than those expected on the basis of water dipolar response. The dielectric amplification is obtained when complete or incomplete C-S-H gel phase barriers block current flow between adjacent capillary pores [25,26].

Mortar is a complex porous material consisting mainly of grain sands, C-S-H gel, calcium silicate CH, unreacted cement, water in capillaries and gel pores as well as absorbed and chemically bonded water. During the hardening process of cement paste, the water has various states of binding, such as chemically bound water associated with silicate layers, water of crystallization associated with calcium hydroxide CH product and physically absorbed water on large-surface area gel C-S-H pores. Structural or chemically bound water has dielectric properties similar to ice, which has a small loss peak near 100 kHz. Free-water relaxation occurs in the frequency range around 10 GHz, while frequencies between 10 and 50 MHz correspond to the relaxation of water molecules which are physically absorbed from the pores [16]. Dispersions in the frequencies 1 and 100 MHz, as a function of curing time, have been identified and attributed to water attached to calcium silicate through hydrogen bonds (100 MHz), or to water attached to calcium silicate by chemical bonds (1 MHz) [14]. According to the above, it seems that a contribution from hydrated water, which is attached to calcium silicate via chemical bonds, should be present in the HF relaxation.

In the frequency range 1 kHz–1 MHz where LF and HF relaxations are present, measurements of complex dielectric permittivity reveal dispersion, as reported also by other researchers [13,17,18]. It has been suggested that this polarization mechanism is due to double-layer relaxation process of ions on the surface of binder particles (fly ash, FA) [17,18], or on the gel surface [13]. After the initial outgrowth of hydration, the contribution $\Delta\varepsilon'$ of the polarization mechanism decreases as a function of hardening time [13,17,18]. The LF relaxation of the present study, at few kHz range, has been observed for the first time, to the best of our knowledge, on cement mortars. The absence of DC conductivity effects, due to the curing conditions of our samples (low relative humidity), makes the LF relaxation detectable. On the other hand, the HF relaxation of the present study exhibits similarities with the low-frequency mechanism of [13], because it appears during the first days of hardening in the same frequency range, 1–10 MHz, while the contribution to the real part $\Delta\varepsilon'$ decreases as a function of hardening time. The main difference of our HF relaxation, as compared to the low-frequency relaxation mechanism of [13], is that the HF mechanism appears to have a relaxation time about two orders of magnitude higher during the whole period of the measurements.

The dependence of the imaginary part of the electric modulus, M'', on frequency is shown in Fig. 3 for several days of hardening. The real and imaginary parts of the electric modulus M^* are related to complex dielectric permittivity components by the following relations: $M' = \varepsilon'/(\varepsilon'^2 + \varepsilon''^2)$ and $M'' = \varepsilon''/(\varepsilon'^2 + \varepsilon''^2)$. In electric modulus formalism the electrode polarization effects, which are usually revealed in ε^* and σ^* formalisms, are suppressed [27]. On the first days of hardening, one peak is observed at a few kHz region which moves to lower frequencies as the hardening time increases. This mechanism corresponds to conductivity relaxation which is dominant during the first hardening days in the low-frequency range (see Fig. 1). As the hardening time increases, a peak appears in the high-frequency range which shifts to lower frequencies.

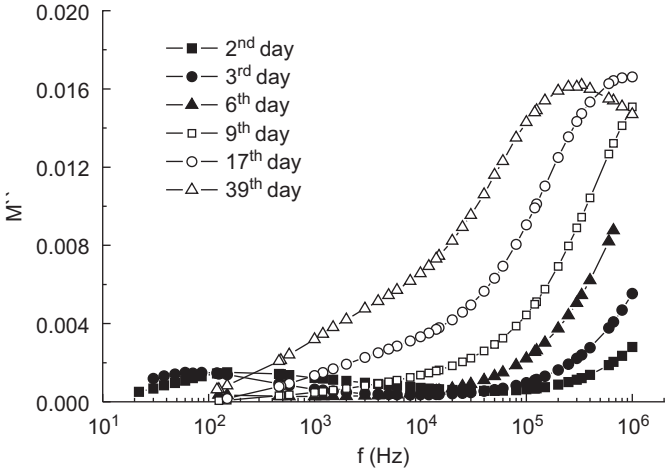

Fig. 3. The imaginary part of the electric modulus versus frequency for several days of hardening.

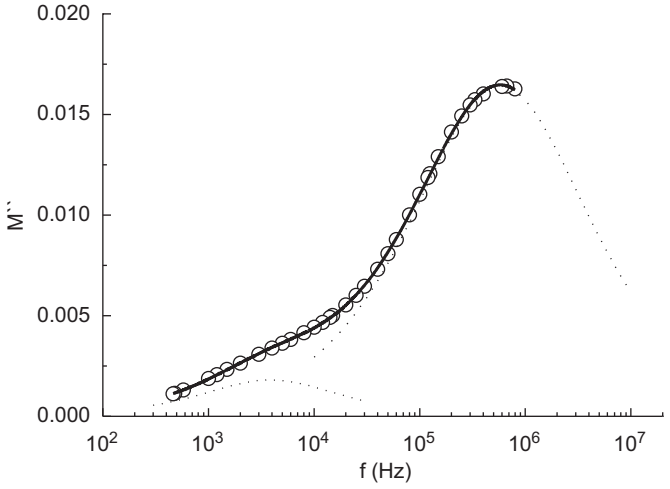

Fig. 4. The imaginary part of the electric modulus versus frequency of cement mortar at 24th day of hardening. The solid line is the best fit according to Eq. (8). The dotted lines show the contribution of the LF and the HF relaxations to the total spectrum.

As we can see in $M'' = M''(f)$ plots of Fig. 3, another relaxation mechanism appears as a shoulder which increases in the low-frequency range, after the first week of hardening. In analogy with the frequency dependence of ε'', the frequency dependence of the imaginary part M'' can be described by the sum of the two empirical Havriliak–Negami model equations [19]

$$M'' = \sum_{i=1}^{2} \mathrm{Im}\left[\frac{\Delta M_i'}{(1 + (\mathrm{i}\omega\tau_{oi})^{1-\alpha_i})^{\beta_i}}\right] \tag{8}$$

where $\Delta M' = M'_\infty - M'_s$, $M'_\infty = 1/\varepsilon'_\infty$, $M'_s = 1/\varepsilon'_s$, $\tau_o = 1/2\pi f_o$, where f_o is a characteristic frequency that is closely related to the frequency that M'' attains a maximum at $f_{M''_{max}}$. In the case of Debye or Cole–Cole shape $f_o = f_{M''_{max}}$. Fig. 4 shows a representative best fit of Eq. (8) to the experimental data of the 24th day of hardening. The fitting parameters of the best fits were calculated in M^* formalism, and they are shown in Table 2.

Both peaks exhibit a Cole–Cole behavior, i.e. they are characterized by a symmetrical distribution of relaxation times. The two peaks which contribute to the total $M'' = M''(f)$ spectrum of Fig. 3 correspond to LF and HF relaxations of $\varepsilon'' = \varepsilon''(f)$ plots (Fig. 1). In the case of a relaxation mechanism with a single

relaxation time (Debye behavior, $\alpha=0$ and $\beta=1$ in H–N expression), the maximum M'' value is defined as $M''_{max}=C_o/2C$, where C is the capacitance associated with the regions where relaxation takes place [27]. So, in the M'' versus f plots, the relaxation mechanism which is associated with the smallest capacitance C is dominant and in our case this is the HF relaxation. In the M^* formalism except the conductivity mechanisms, other polarization mechanisms (i.e. from dipoles or ions) are also detected. This is due to the fact that the capacitances corresponding to the polarization mechanisms do not differ significantly from those corresponding to conductivity relaxation mechanisms [24].

The dependence of $\log Z''$ versus $\log f$ seems to be almost linear after the first week of hardening. This is related to the fact that the resistance which is associated to the LF and HF relaxations attains small values, thus, the contribution of the electrode/sample effects is screening the above mechanisms. Constant phase elements (CPE) are empirical functions responding in the form $Z^*(\mathrm{CPE})=A(i\omega)^{-n}$, where A is constant and n is a parameter having values between -1 and 1. In the case of $n=1$ the CPE impedance represents a capacitor, when $n=0$ it represents a resistor and if $n=-1$ it represents an inductor. CPE usually describes the electrode/sample response. The imaginary component of CPE impedance is the following:

$$Z''(\mathrm{CPE})=\left[(2\pi)^{-n}A\sin\left(\frac{n\pi}{2}\right)\right]f^{-n} \quad (9)$$

The experimental data of Z''–f do not fit with Eq. (9). Thus, the following expression was fitted to the experimental data:

$$Z''(f)=Bf^{-n}+\sum_{i=1}^{2}\mathrm{Im}\left[\frac{R_i}{[1+(i\omega\tau_{oi})^{1-\alpha_i}]^{\beta_i}}\right] \quad (10)$$

which comprises the sum of two H–N equations and one CPE impedance component corresponding to the electrode/sample contribution. R is the resistance related to each relaxation mechanism (LF and HF) and $B=(2\pi)^{-n}A\sin(n\pi/2)$. Fig. 5 shows the best fit of Eq. (10) to the experimental data of the 24th day of hardening. The same figure shows the contribution of each relaxation mechanism to the total spectrum. The fitting parameters of the best fits were calculated following the Z^* formalism, and they are shown in Table 3.

Inside Fig. 5 the equivalent circuit, which describes the response of the two relaxation mechanisms and electrode/sample interfaces, is presented. The n values around 0.9 indicate a predominantly capacitive behavior of the electrode/sample interface. LF and HF relaxations exhibit a symmetrical Cole–Cole shape in both formalisms, Z^* and M^*, as shown in Tables 2 and 3. This means that the LF and HF relaxations are characterized by symmetrical distribution of relaxation times, in these formalisms. Each relaxation, LF and HF, presents a maximum in ε^*, M^* and Z^* formalisms which follows the order $f_{M'',max}\geq f_{Z'',max}>f_{\varepsilon'',max}$, as expected [28].

The hardening process within the cement mortar can be described as follows. In the early stages, the capillary pores create percolative paths which contribute to the DC conductivity of the cement sample. As hardening time increases, C-S-H gel barriers block the connectivity of capillary pores and generate gradually individual pores which contain an ionic solution. On the other hand, due to the fact that the C-S-H gel phase continuously grows, it results in the generation of nanometric isolated pores within this phase, also containing ionic solution. When the cement samples are stored in a low relative humidity environment (as in our case), then the hydration reaction is slower than that of samples cured in high relative humidity environment. The reaction products, during the hardening process, increase gradually the ionic content of capillary pores [29]. Thus, ionic solution exists mainly in capillary pores and C-S-H gel pores during the hardening period. We suggest that the mechanisms detected in both Z^* and M^* formalisms be related to the short-range conductivity relaxations which take place in the pore regions. The LF relaxation is connected to the closed capillary pores of larger size (higher relaxation time or lower frequency peak). The HF relaxation is connected to the C-S-H gel pores of smaller size (lower relaxation time or higher frequency peak).

During the first days of hardening the DC conductivity effects dominate in the lower frequency range in all DS formalisms. In addition, one relaxation mechanism also appears at frequencies higher than 1 MHz. The contribution from hydrated water is normally expected to be present in the high-frequency relaxation

Table 2
The parameters of the best fits of Eq. (8).

Day	α_L	β_L	f_{oL} (kHz)	$\Delta M'_L$	α_H	β_H	f_{oH} (kHz)	$\Delta M'_H$
17	0.22	1	4.65	0.0043	0.28	1	747.02	0.0515
24	0.19	1	3.85	0.0049	0.32	1	583.89	0.0562
39	0.06	1	2.02	0.0041	0.41	1	333.54	0.0655

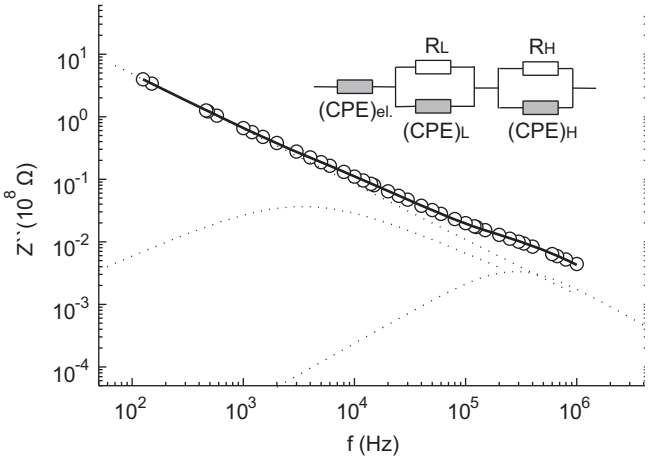

Fig. 5. The imaginary part of the complex impedance versus frequency of cement mortar at 24th day of hardening. The solid line is the best fit according to Eq. (10). The dotted lines show the contribution of the electrode–sample effects as well as the contribution of the LF and HF relaxations to the total spectrum. Inside, the equivalent circuit, which describes the response of the two relaxation mechanisms and electrode–sample interfaces, is presented.

Table 3
The parameters of the best fits of Eq. (10).

Day	α_L	β_L	f_{oL} (kHz)	R_L (MΩ)	α_H	β_H	f_{oH} (kHz)	R_H (MΩ)	B ($\times 10^6$)	n
14	0.11	1	5.83	3.4	0.05	1	314.57	0.63	3.22	0.91
17	0.18	1	3.63	6.7	0.05	1	300.71	0.65	3.12	0.90
24	0.21	1	3.40	10.0	0.03	1	280.07	0.67	2.80	0.88
39	0.23	1	1.55	24.5	0.05	1	129.98	1.10	2.29	0.84

[14]. After the first week of hardening the DC conductivity effects are absent. Bearing in mind that the DC conductivity is due to ion motion in percolative capillary pores channels, we expect that the observed reduction of conductivity is a result of the C-S-H gel barriers which block the connectivity of such pores. This phenomenon generates gradually individual pores and leads to an increase of dielectric amplification effects in the lower frequency range, which are manifested by the gradual increase of $\varepsilon''_{\max}$ values of the LF relaxation. The reaction products, which increase slowly the ionic content of closed capillary pores, have as a result the increase of the dielectric loss of the LF relaxation. As hardening time elapses, the continuous growth of C-S-H gel phase is expected to reduce the volume fraction of C-S-H gel pores. This explains the observed gradual reduction of the dielectric loss of the HF relaxation, after the first week of hardening.

The ionic solution within closed capillary pores and C-S-H gel pores is characterized by short-range conductivity relaxation mechanisms. These relaxations correspond to LF and HF relaxations, respectively, in Z^* and M^* formalisms. Information derived from Z^* and M^* is related to the resistances and capacitances that are related to LF and HF relaxations. As shown in Table 3, the R_L values increase gradually with hardening time. This is attributed to the increase of the volume fraction of the closed capillary pores. The increase of the volume fraction reflects also an increase of $M''_{\max}$ value (see Fig. 3) because the associated capacitance of the particular LF relaxation decreases [30]. On the other hand, we expected a reduction of R_H values as a result of the decrease of the C-S-H gel pores volume fraction. However R_H values present small increases as a function of hardening time (Table 3). This should be attributed to an increase in resistivity of the particular regions within the sample [30]. The electric modulus formalism M^* is a more convenient one to represent the relaxation of the electric field **E**, under the constraint of a constant displacement vector **D**, because $\mathbf{E} = M^*\mathbf{D}$. The shape parameters α_i in M^* formalism have values greater than 0, as presented in Table 2. This implies that the LF and HF relaxations are characterised by a distribution in relaxation times which reflects the distribution of pore diameters. As shown in Table 2, the value of shape parameter α_L of LF relaxation decreases as a function of hardening time. This indicates a narrowed distribution of relaxation times and also a narrowed distribution of capillary pores dimension. On the other hand, the value of shape parameter α_H of HF relaxation increases as a function of hardening time. This indicates a broader distribution of relaxation times and also a broader distribution of C-S-H gel pore dimensions.

In order to approximate the capacitances which are connected to LF and HF relaxations, we assumed that both relaxations are characterized by a single relaxation time, the mean relaxation time $\tau = 1/(2\pi f_{M''_{\max}})$. In this case the equivalent circuit is the one shown in Fig. 5, provided that the complex elements $(CPE)_L$ and $(CPE)_H$ are substituted by the pure capacitances C_L and C_H. Thus, each relaxation is described by the time constant $\tau_i = R_i C_i$. Finally, the capacitances related to LF and HF relaxations can be estimated through relation $C_i = 1/2\pi R_i f_{M'',\max}$, while for values of R_i, Table 3 is used. Calculations give C_L values: 5.1, 4.1 and 3.2 pF for 17, 24 and 39 days of hardening, respectively. C_H values are 0.32 pF, 0.40 pF and 0.44 pF for the same days of hardening respectively. It must be mentioned here that the above estimations for the C_L and C_H values are consistent with the discussion of the previous paragraph. The increase of the volume fraction of closed capillary pores, as a function of hardening time, leads to a decrease of C_L values. The decrease of volume fraction of the C-S-H gel pores, as a function of hardening time, leads to increase of C_H values.

The ionic motion induced by the applied electric field will have a time constant $\tau = \delta^2/D$ [31], where δ represents the effective path distance (the pore diameter in our case) and D is the average diffusion coefficient of the ionic species involved (Ca^{2+}, Na^+, K^+, OH^-). The values of the diffusion coefficient for the different ionic species depend on the concentration, which is of the order of 10^{-5} cm^2/s. An estimation of the mean pore diameter, deduced from the previous relation, can be made by assuming a mean relaxation time of $\tau = 1/2\pi f_{M''_{\max}}$ for each relaxation ($f_o = f_{M''_{\max}}$ from Table 2). The estimation yields the mean C-S-H gel pores, 15, 17 and 22 nm for the days 17, 24 and 39, respectively. These values are very close to those of [2] for C-S-H gel pores. Evaluations of the mean capillary pores give 186, 203 and 282 nm after 17, 24 and 39 days, respectively. It should be noted here that mercury intrusion results on cement samples of similar w/c ratio present two peaks close to 20 and 200 nm [32]. Mercury intrusion measurements approximate better the dimension of capillary pores [4]. A gradual increase of the mean dimensions is observed in both capillary pores and C-S-H gel pores, based on the previous estimations.

3.2. Isothermal depolarization current technique

Fig. 6 demonstrates the recorded values of the isothermal depolarization currents in log–log plot with respect to time during the cement hardening process. Specifically, the log–log plot contains five curves corresponding to the 3rd, 4th, 7th, 14th and 39th day of the hardening process. The initial obvious results are the following: Time response of the decay current for all samples

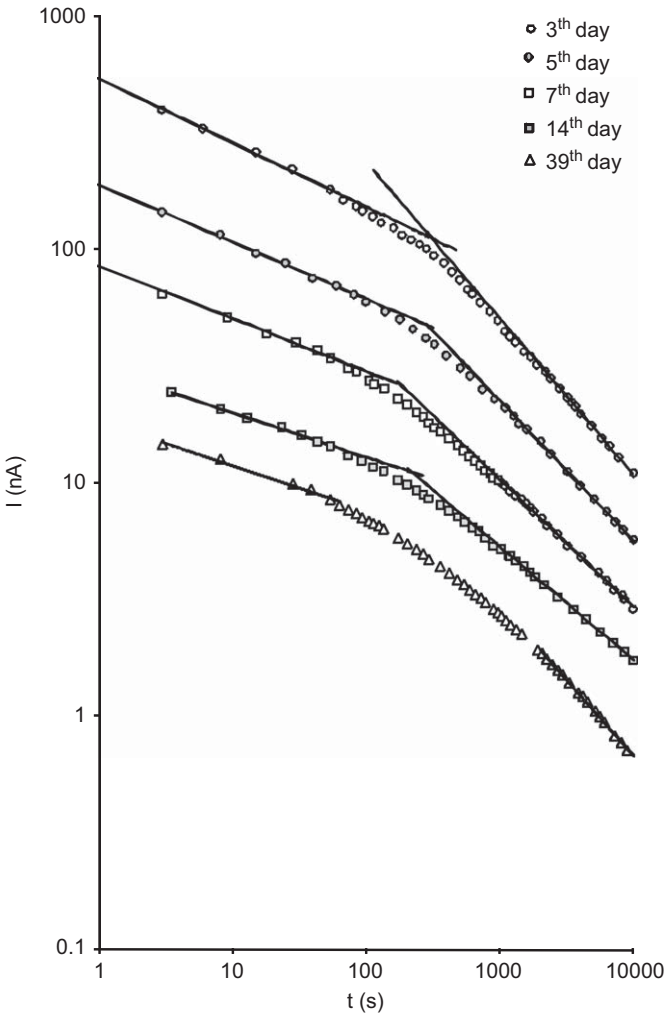

Fig. 6. Depolarization currents in log–log plot for the cement mortar for several days of hardening.

was characterized by two distinct branches of different slopes $-n$ and $-(m+1)$. The near-Debye process describes the transition part between the two branches. When the IDC curve was measured during the first days, it was found that significantly higher IDC values were recorded. The form of all recorded IDC is the same.

It is important to notice the influence of the hardening process and the subsequent water content and chemical processes involving the values of the two factors (n and m) that describe depolarization stages. The values of the factor n that describe the flip depolarization mechanisms [21] and correspond to the "short" times (i.e. second depolarization stage) do not exhibit major variations for all measurements (see Fig. 7). Additionally, the values of the n factor are continuously decreasing. The values of the factor m that describes the flip–flop depolarization mechanisms [21] and correspond to "long" time (i.e. the fourth stage of the depolarization process) vary considerably depending on the day of hardening. Additionally, the m factor seems to attain different behaviors during the hardening process while during the first 14 days factor m increased and then decreased again to achieve its initial value on the 22nd day.

The curves of Fig. 6 also manifest that the flip transition duration does not vary with time, since during the entire hardening process they do not provide any sign of change proving that the fast mechanisms remain active and dominant for the first 100 s even after 39 days of hardening. The same observation cannot be made for the m factor since it gradually initiates, making the transition between flip and flip–flop mechanisms longer.

The values of the two factors seem to stop varying after the 22nd day of the hardening process. This can be attributed to the chemical processes that are completed by then and to the fact that the included water has already been absorbed or transformed into other chemical products. The high water content that initially exists in the cement sample bulk can explain the higher IDC in the very first days. Gradually the water evaporates; it is captured in the sample capillaries and forms the cement mortar product. In any case it is eliminated in the sample. This limits the fast depolarization processes "flip" transitions while the influenced dipoles become localized in the sample bulk. The slow, "flip–flop" transitions are actually influenced by the fast transitions. The increasing–decreasing behavior of the m factor can be attributed to the two factors that influence this slow process.

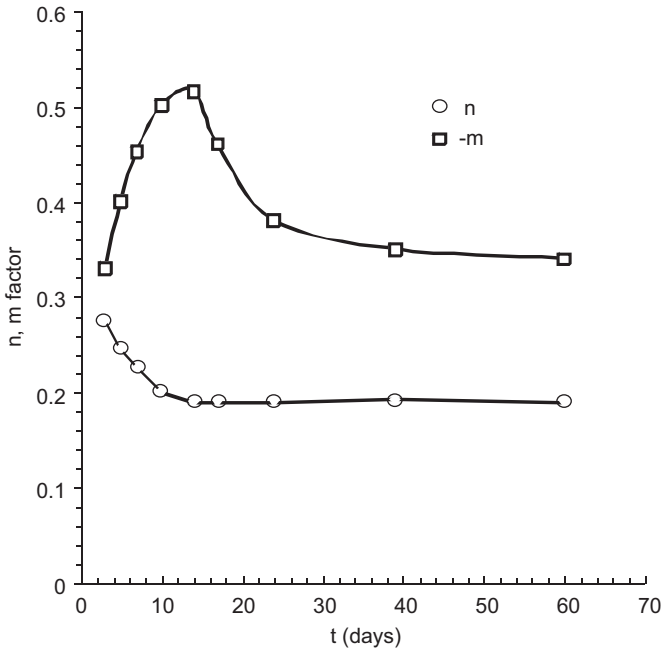

Fig. 7. The exponents m and n as a function of the hardening time.

The first factor is the gradually limiting water content in the sample and the second factor is the sand–cement interfaces. These are the two parameters that continuously change during hardening. Since during the first 14 days the dominant factor is the continuous decrease of the water content, this is expected to influence both n and m factors. It must also be noted that both fast and slow depolarization processes exist continuously during the IDC recording but each dominates for a different time. Specifically, the fast depolarization processes decrease gradually since they are not favored in an environment of limited water content. The smaller the number of fast transitions, the less is the probability for them to cause slow transition due to interaction. After 14 days the water is almost absorbed and it is located in free form only in the closed capillary and C-H-S gel pores. Thus, the n factor describing the fast depolarization process becomes stabilized but the slow depolarization mechanisms that can be affected by the chemical processes are enforced and regain their initial values.

4. Conclusions

The present study deals with the dielectric and electrical properties of cement mortar samples, cured at low relative humidity environment. Measurements were made by using dielectric spectroscopy over a broad frequency range of 20 Hz–1 MHz, and the isothermal depolarization currents technique during the hardening process for several weeks.

During the first week of hardening, the DC conductivity effects were dominant. One dielectric relaxation mechanism appeared during the first days at frequencies higher than 1 MHz, which gradually shifted to lower frequencies as the hardening time increased. After the first week, two distinct relaxation mechanisms existed in the frequency spectrum, in ε^* and $\tan\delta$ formalisms, both of which shifted to lower frequencies with time. The dielectric strength of the low-frequency mechanism increased with time, while the relaxation mechanism at the high frequency decreased. The low-frequency relaxation was observed for the first time, at few kHz region, on cement mortars.

Fitting analysis in Z^* and M^* formalisms revealed the existence of two short-range conductivity relaxation mechanisms, which correspond to the low- and high-frequency relaxations of ε^* and $\tan\delta$ formalisms. Taking into account the electrochemical processes occurring within the cement mortar, we suggest that the low-frequency relaxation is related to the closed capillary pores and the high-frequency relaxation to the C-S-H gel pores. A contribution from hydrated water attached to calcium silicate via chemical bonds cannot be excluded. Estimations of the mean diameters give values around 20 nm for C-S-H gel pores and around 200 nm for the closed capillary pores, during the first month of hardening. The mean pore dimensions were found to increase with the hardening time.

In the light of the IDC results, the following conclusions can be drawn. During the first days of hardening the depolarization currents are high and become gradually low while hardening proceeds. The behaviors of the two transition mechanisms have also been studied and it was found that both factors n and m are influenced by this process for only the first 2 weeks after sample preparation.

Acknowledgment

The authors would like to thank Dr. P. Photopoulos for the helpful discussion.

References

[1] F.W. Taylor, Cement Chemistry, Academic Press, New York, 1990, pp. 167–232.
[2] M. Cabeza, P. Merino, X.R. Novoa, I. Sanchez, Electrical effects generated by mechanical loading of hardened Portland cement paste, Cem. Concr. Compos. 25 (2003) 351–356.
[3] B.J. Christensen, T.O. Mason, H.M. Jennings, Influence of silica fume on the early hydration of Portland cements using impedance spectroscopy, J. Am. Ceram. Soc. 75 (1992) 939–945.
[4] G.U. Ping, J.J. Beaudoin, Dielectric behaviour of hardened cementitious materials, Adv. Cem. Res. 33 (1997) 1–8.
[5] W.J. McCarter, G. Starrs, T.M. Chrisp, Immittance spectra for Portland cement/fly-ash-based binders during early hydration, Cem. Concr. Res. 29 (1999) 377–387.
[6] G. Song, Equivalent circuit model for AC electrochemical impedance spectroscopy of concrete, Cem. Concr. Res. 30 (2000) 1723–1730.
[7] S.S. Yoon, H.C. Kim, R.M. Hill, The dielectric response of hydrating porous cement paste, J. Phys. D: Appl. Phys. 29 (1996) 869–875.
[8] V. Saltas, F. Vallianatos, D. Triantis, Dielectric properties of non-swelling bentonite: the effect of temperature and water saturation, J. Non-Cryst. Solids 354 (2008) 5533–5541.
[9] A. Zerwer, J.C. Santamarina, Double layers in pyrometamorphosed bentonite: index properties and complex permittivity, Appl. Clay Sci. 9 (4) (1994) 283–291.
[10] J.R. Macdonald, W.B. Johnson, Impedance Spectroscopy: Emphasizing Solid Materials and Systems, Wiley, New York, 1987.
[11] C.A. Scuderi, T.O. Mason, H.M. Jennings, Impedance spectra of hydrating cement pastes, J. Mater. Sci. 26 (1991) 349–353.
[12] G.A. Niklasson, A. Berg, K. Brantervik, B. Hedberg, L.O. Nilsson, Dielectric properties of porous cement mortar: fractal surface effects, Solid State Commun. 79 (1991) 93–96.
[13] N.E. Hager, R.C. Domszy, Monitoring of cement hydration by broadband time-domain-reflectometry dielectric spectroscopy, J. Appl. Phys. 96 (2004) 5117–5128.
[14] N. Miura, N. Shinyashiki, S. Yagihara, M. Shiotsubo, Microwave dielectric study of water structure in the hydration process of cement paste, J. Am. Ceram. Soc. 81 (1998) 213–216.
[15] Y. Hafiane, A. Smith, P. Abelard, J.P. Bonnet, P. Blanchart, Dielectric characterization at high frequency (1 MHz–1.8 GHz) of a Portland cement at the early stages of hydration, Ceramics—Silikaty 43 (1999) 48–51.
[16] Y.E. Hafiane, A. Smith, J.P. Bonnet, P. Abelard, P. Blauchart, Electrical characterization of aluminous cement at early age in the 10 Hz–1 GHz frequency range, Cem. Concr. Res. 30 (2000) 1057–1062.
[17] W.J. McCarter, T.M. Chrisp, G. Starrs, J. Blewett, Characterization and monitoring of cement-based systems using intrinsic electrical properties measurements, Cem. Concr. Res. 33 (2003) 197–206.
[18] W.J. McCarter, G. Starrs, T.M. Chrisp, The complex impedance response of fly-ash cements revisited, Cem. Concr. Res. 34 (2004) 1837–1843.
[19] C.J.F. Bottcher, P. Bordewijk, Theory of Electric Polarization, vol. II, Elsevier, Amsterdam, 1978, p. 72.
[20] E. Neagu, Combined isothermal and nonisothermal dc measurements to analyze space-charge behaviour in dielectric materials, J. Appl. Phys. 97 (4) (2005) 1–9.
[21] A.K. Jonscher, Dielectric Relaxation in Solids, Chelsea Dielectric, 1996, p. 282.
[22] L.A. Dissado, R.M. Hill, The fractal nature of the cluster model dielectric response functions, J. Appl. Phys. 66 (1989) 2511–2524.
[23] C.E. Anastasiadis, I.D. Stavrakas, D.A. Triantis, A.D. Kyriazopoulos, K.D. Ninos, Rock damage estimation with dielectric loss ($\tan\delta$) measurements, Int. J. Microstruct. Mater. Prop. 1 (2006) 421–429.
[24] C. Tsonos, L. Apekis, K. Viras, L. Stepanenko, L. Karabanova, L. Sergeva, Electrical and dielectric behavior in blends of polyurethane-based ionomers, Solid State Ion. 143 (2001) 229–249.
[25] R.T. Coverdale, B.J. Christensen, T.O. Mason, H.M. Jennings, E.J. Carboczi, Interpretation of the impedance spectroscopy of cement paste via computer modeling. II: Dielectric response, J. Mater. Sci. 29 (1994) 4984–4992.
[26] S.J. Ford, J.H. Hwang, J.D. Shane, R.A. Olson, G.M. Moss, H.M. Jennings, T.O. Mason, Dielectric amplification in cement pastes, Adv. Cem. Bas. Mater. 5 (1997) 41–48.
[27] P.B. Macedo, C.T. Moynihan, R. Bose, The role of ionic diffusion in polarizationin vitreous ion conductors, Phys. Chem. Glasses 13 (1972) 171–179.
[28] W. Cao, R. Gerhardt, Calculation of various relaxation times and conductivity for a single dielectric relaxation process, Solid State Ion. 42 (1990) 213–221.
[29] C. Andrade, V.M. Blanco, A. Collazo, M. Keddam, X.R. Novoa, H. Takenouti, Cement paste hardening processing studied by impedance spectroscopy, Electrochim. Acta 4 (1999) 4313–4318.
[30] D.C. Sinclair, A.R. West, Effect of atmosphere on the PTCR properties of $BaTiO_3$ ceramics, J. Mater. Sci. 29 (1994) 6061–6068.
[31] C. Alonso, C. Andrade, X.R. Novoa, M. Keddam, H. Takenouti, Study of the dielectric characteristics of cement paste, Mater. Sci. Forum 289–292 (1998) 15–28.
[32] R.A. Cook, K.C. Hover, Mercury porosimetry of hardened cement pastes, Cem. Concr. Res. 29 (1999) 933–943.